New Journal of Physics
The open access journal at the forefront of physics
Deutsche Physikalische Gesellschaft DPG | IOP Institute of Physics

Orbital symmetry fingerprints for magnetic adatoms in graphene

Bruno Uchoa[1,2,7], **Ling Yang**[3], **S-W Tsai**[3], **N M R Peres**[4] **and A H Castro Neto**[5,6]

[1] Department of Physics and Astronomy, University of Oklahoma, 440 West Brooks Street, Norman, OK 73019, USA
[2] Department of Physics, University of Illinois at Urbana-Champaign, 1110 West Green Street, Urbana, IL 61801, USA
[3] Department of Physics and Astronomy, University of California, Riverside, CA 92521, USA
[4] Centro de Física e Departamento de Física, Universidade do Minho, P-4710-057 Braga, Portugal
[5] Graphene Research Centre, and Department of Physics, National University of Singapore, 2 Science Drive 3, Singapore 117542, Singapore
[6] Department of Physics, Boston University, 590 Commonwealth Avenue, Boston, MA 02215, USA
E-mail: uchoa@nhn.ou.edu

Received 4 October 2013, revised 6 December 2013
Accepted for publication 12 December 2013
Published 23 January 2014
New Journal of Physics **16** (2014) 013045
doi:10.1088/1367-2630/16/1/013045

Abstract

In this paper, we describe the formation of local resonances in graphene in the presence of magnetic adatoms containing localized orbitals of arbitrary symmetry, corresponding to any given angular momentum state. We show that quantum interference effects which are naturally inbuilt in the honeycomb lattice in combination with the specific orbital symmetry of the localized state lead to the formation of fingerprints in differential conductance curves. In the presence of Jahn–Teller distortion effects, which lift the orbital degeneracy of the adatoms, the orbital symmetries can lead to distinctive signatures in the local density of states. We show that those effects allow scanning tunneling probes to characterize adatoms and defects in graphene.

[7] Author to whom any correspondence should be addressed.

1. Introduction

Graphene is a single atomic layer of graphite whose low energy quasi-particles behave as massless Dirac fermions [1–3]. As an open surface, graphene offers a solid playground for the detection and local manipulation of quantum states with scanning tunneling (STM) probes. This perspective is particularly promising for adatoms, which can be dragged with atomic precision [4] and can have their magnetic state monitored and controlled with the application of an external gate voltage [5, 6]. There has been substantial progress in the quality of the STM experiments in graphene in the last few years [7–16]. Recent experiments reported the observation of Landau levels spontaneously generated by strain on the top of nanobubbles in graphene [17], and the observation of charge polarization effects around a Co adatom [18].

Although the microscopic theory of STM is well understood in metallic hosts [19, 20], in graphene the sublattice quantum numbers play a role in the interference effects that drive the emergence of Fano resonances [21] nearby adatoms, in the presence of an STM tip. In particular, for adatoms that sit at the center of the honeycomb hexagon (H site), destructive interference between the different electronic paths of hybridization with the two sublattices may give rise to a suppression of the Fano resonance of the localized state [22–24], and also change the scattering rate of the localized electrons due to the presence of the fermionic bath [22]. In general, the broadening of a localized state, magnetic or not, is expected to scale as $\Delta(\omega) \propto |\omega|^r$, where r is the scaling dimension of the density of states (DOS) of the host material, which in graphene is $r = 1$ ($r = 0$ for metals). In graphene, nevertheless, localized orbitals located either in substitutional impurity sites (S sites) or in H sites and which also preserve the C_{3v} point group symmetry of each sublattice are effectively damped at low energies by a fermionic bath with $r = 3$ [22, 25], due to quantum interference effects. This effect suggests that the local density of states (LDOS) can by quite susceptible to the orbital symmetry of the localized state, allowing STM probes to characterize adatoms and defects in graphene.

In this work, we describe in detail the effect of the localized orbital symmetry in the emergence of local magnetic resonances near the adatoms with inner shell electrons. We discuss the emergence of non-trivial particle-hole asymmetries in the energy dependence of the level broadening $\Delta(\omega)$, depending on the particular symmetry and position of the localized state in the lattice. We also describe the way the differential conductance curves reflect the orbital symmetry of spin polarized states.

In real crystals, where the adatoms are randomly distributed, local lattice distortions created by the adatoms [26] can displace them from high symmetry positions in the crystal. In the presence of local Jahn–Teller distortions that lift orbital degeneracies, we also show that the adatoms can induce distinctive signatures of the individual orbital symmetries directly in the LDOS of graphene, which can be measured with local energy resolved spectroscopy experiments. This effect is not present in ordinary host metals. We will address the limiting situation where the charge of the orbitals in a given irreducible representation is strongly polarized. In graphene, where orbital degeneracies appear in the form of doublet states, this limit can be physically described by adatoms with total spin $1/2$, when one of the orbitals in the doublet is half filled (spin polarized) and the other empty. In this regime, which will be assumed for most of the paper, the problem can be described by an effective *single* orbital Hamiltonian. In the second part of the paper, we address the theory of scanning tunneling spectroscopy developed in [22] for the case of s-wave orbitals, and generalize it to describe higher angular momentum states in the case of interest, for adatoms with total spin near $1/2$.

The outline of the paper is as follows: in section 2, we describe the generic zero-dimensional Hamiltonian of an adatom in graphene; in section 3 we briefly describe the role of the orbital symmetry into the formation of local magnetic moments and we show the manifestation of those orbital symmetries in the LDOS, whenever the adatom hybridizes with two or more carbon atoms. We address in particular the appearance of particle–hole asymmetries in the level broadening observed in *ab initio* calculations. In section 4 we address the STM tip effects in the LDOS and we compute the differential conductance accounting for the symmetry of the localized orbitals and their position with respect to the sublattices. Finally, in section 5 we present our conclusions.

2. Hamiltonian

The Hamiltonian of a magnetic adatom in graphene is described by a sum of four terms

$$H = H_g + H_f + H_V + H_U, \tag{1}$$

where

$$H_g = -t \sum_{\langle ij \rangle} a^\dagger_\sigma(\mathbf{R}_i) b_\sigma(\mathbf{R}_j) + \text{h.c.} \tag{2}$$

is the graphene Hamiltonian in tight-binding, with $t \sim 2.8$ eV the hoping energy between nearest neighbors sites, a (b) is a fermionic annihilation operator in the A (B) sublattice, with $\sigma = \uparrow, \downarrow$ indexing the spin. In momentum space,

$$H_g = -t \sum_{\mathbf{p}\sigma} \left(\phi_{\mathbf{p}} a^\dagger_{\mathbf{p}\sigma} b_{\mathbf{p}\sigma} + \text{h.c.} \right), \tag{3}$$

where $\phi_{\mathbf{k}} = \sum_{i=1}^{3} e^{i\mathbf{k}\mathbf{a}_i}$ and $\mathbf{a}_1 = \hat{x}$, $\mathbf{a}_2 = -\hat{x}/2 + \sqrt{3}\hat{y}/2$ and $\mathbf{a}_3 = -\hat{x}/2 - \sqrt{3}\hat{y}/2$ are the lattice nearest-neighbor vectors. The second term

$$H_f = \sum_\sigma \sum_m \epsilon_0 \, f^\dagger_{m,\sigma} f_{m,\sigma} \tag{4}$$

is the Hamiltonian of the localized level with energy ϵ_0 measured from the Dirac point, with m the angular momentum projection indexing the different degenerate orbitals contained in a given irreducible representation with angular momentum l (for instance, the doublets d_{xy}, $d_{x^2-y^2}$, with $l = 2$ and $m = \pm l$). In graphene, due to the three-fold rotational symmetry of each sublattice, the crystalline filed anisotropy lifts the degeneracy of the orbitals for different values of $|m| \leqslant l$, leaving pairs of degenerate states (doublets) with angular momentum projections $\pm|m|$ with $m \neq 0$.

The third term in equation (1) gives the hybridization Hamiltonian. When the adatoms sit on top of a carbon atom as in the case of H and F atoms, and also simple molecules [28] such as NO_2,

$$H_V = V \sum_{\sigma,m} a^\dagger_\sigma(0) \, f_{m,\sigma} + \text{h.c.}$$

for adsorption on a given site, say on sublattice A. Adatoms such as transition metals may instead strongly prefer to sit in the hollow site [29] at the center of the hexagon in the

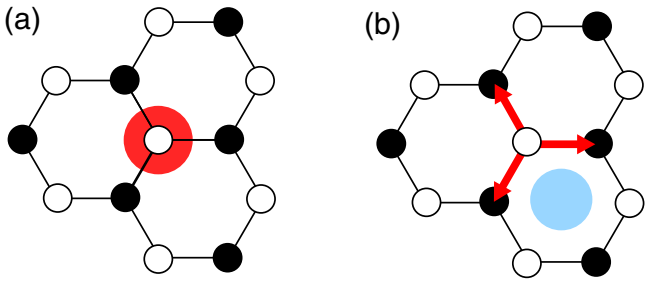

Figure 1. Honeycomb lattice in graphene, with two distinct sublattices (black and white circles). (a) Adatom siting on top of a carbon atom on sublattice A and (b) sitting in the center of the honeycomb hexagon. Red arrows: nearest-neighbor vectors.

honeycomb lattice (see figure 1). In that case, the level is coupled to the graphene bath though the hybridization Hamiltonian [22]

$$H_V = \sum_{\sigma,m} \sum_{i=1}^{3} \left[V_{a,i}^{(m)} a_\sigma^\dagger(\mathbf{a}_i) + V_{b,i}^{(m)} b_\sigma^\dagger(-\mathbf{a}_i) \right] f_{m,\sigma} + \text{h.c.}, \tag{5}$$

where $V_{x,i}$ $(x = a,\ b)$ are the hybridization amplitudes of the adatom with each of the nearest-neighbors carbon atoms, which are set by the orbital symmetry of the localized state. In momentum space representation, this Hamiltonian can be written as [22, 25]

$$H_V = \frac{1}{\sqrt{N}} \sum_{m,\mathbf{p}\sigma} \left(V_{b,\mathbf{p}}^{(m)} b_{\mathbf{p}\sigma}^\dagger + V_{a,\mathbf{p}}^{(m)} a_{\mathbf{p}}^\dagger \right) f_{m,\sigma} + \text{h.c.}, \tag{6}$$

where

$$V_{b,\mathbf{p}}^{(m)} = \sum_{\langle j \rangle} V_{b,j}^{(m)} e^{i\mathbf{p}\mathbf{a}_j}, \tag{7}$$

$$V_{a,\mathbf{p}}^{(m)} = \sum_{\langle j \rangle} V_{a,j}^{(m)} e^{-i\mathbf{p}\mathbf{a}_j} \tag{8}$$

with $\langle j \rangle$ representing summation over the hybridization amplitudes of the adatom with the nearest-neighbor carbon atoms on a given sublattice and N is the number of lattice sites in the extended unit cell of the adatom. The discrete sum over momenta can be interchanged by a continuous integration, $\frac{1}{N}\sum_{\mathbf{k}} \longrightarrow A \int d\mathbf{k}$, where $A = 2/D^2$, where $D \approx 7\,\text{eV}$ is the bandwidth. For notational reasons, we will set $N = 1$ from now on.

For adatoms that sit on top of the carbon atoms (such as hydrogen), $V_{a,\mathbf{p}} = V$ and $V_{b,\mathbf{p}} = 0$, for adsorption on top of an A site and $V_{a,\mathbf{p}} = 0$ and $V_{b,\mathbf{p}} = V$ for a B site. When the adatom sits at the center of the honeycomb hexagons (H site), the strengths of hybridization with the six nearest carbon atoms in the tight-binding description depend explicitly on the symmetry of the orbital: for example, for s-wave orbitals, $V_{x,i} \equiv V$ by symmetry, whereas for in-plane f-wave orbitals, the hybridization amplitudes are anti-symmetric on the two sublattices, $V_{a,i} = -V_{b,i} = V$. In the first case (s-wave), $V_{a,\mathbf{p}} = V\phi_{\mathbf{p}}^*$ and $V_{b,\mathbf{p}} = V\phi_{\mathbf{p}}$ whereas in the second (f-wave) $V_{a,\mathbf{p}} = V\phi_{\mathbf{p}}^*$ and $V_{b,\mathbf{p}} = -V\phi_{\mathbf{p}}$. In the case of a $d_{x^2-y^2}$ orbital $V_{x,1} = V$, $V_{x,2} = V_{x,3} = -V/2$, whereas for a d_{xy} orbital, $V_{x,1} = 0$ and $V_{x,2} = -V_{x,3} = V$ and so on, as illustrated in figure 2.

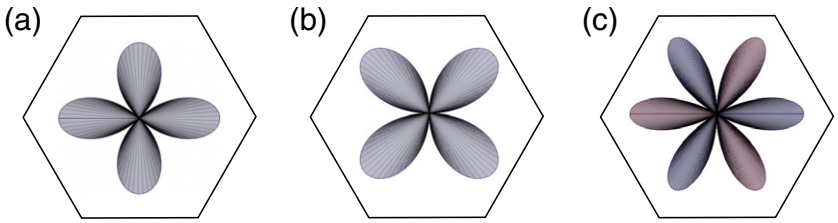

Figure 2. Illustration of d- and f-wave localized orbitals for an adatom that sits at the center of the honeycomb lattice hexagon (H site). (a) $d_{x^2-y^2}$ orbital, that corresponds to hybridization amplitudes $V_{x,1} = V$ and $V_{x,2} = V_{x,3} = -V/2$ with the six nearest-neighbor carbon atoms on sublattices $x = a$, b, at the vertexes of the hexagon (see equations (7) and (8)). (b) d_{xy} orbital corresponding to $V_{x,1} = 0$ and $V_{x,2} = -V_{x,3} = V$. (c) $f_{x(x^2-3y^2)}$ orbital, with hybridization amplitudes $V_{a,i} = -V_{b,i} = V$. Adatoms on top carbon sites and adatoms in H or S sites with p-wave, d-wave and out of plane f-wave orbitals explicitly break the C_{3v} sublattice symmetry in graphene (type I orbitals). s-wave and in-plane f-wave orbitals sitting on H or S sites are C_{3v} invariant (type II orbitals, see text).

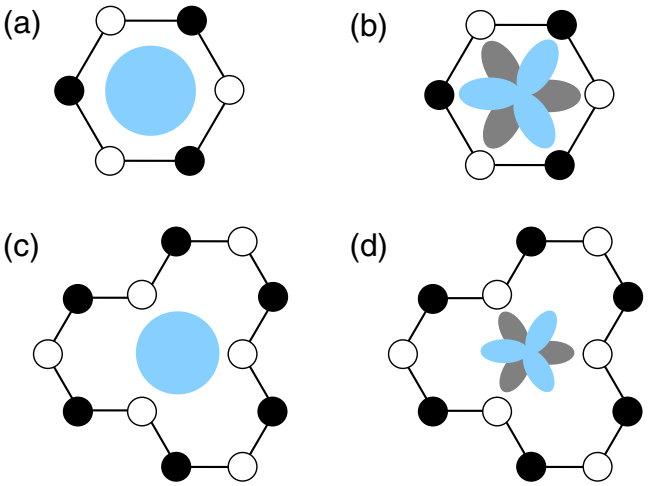

Figure 3. C_{3v} invariant orbitals for adatoms sitting in the center of the hexagon, on H sites (top) and in substitutional (S) sites (bottom). On the left: s-wave orbitals, with zero angular momentum ($m = 0$); on the right: in-plane f-wave orbitals ($m = \pm 3$). In the two cases, the adatoms hybridize equally with the carbon atoms on the same sublattice.

Other interesting cases include for instance substitutional impurities (S-sites) [30], where $V_{a,i} = 0$ for adatoms sitting on A sites and $V_{b,i} = 0$ for substitutional adatoms on B sites (see figure 3). A similar description can be for instance applied for adatoms sitting on bond sites in between two neighboring carbon atoms.

Finally, the last term in equation (1) includes the Coulomb energy (U) and exchange energy (J) for the electrons in the different orbitals [27],

$$H_U = \frac{1}{2}\sum_{\sigma}\sum_{m',m\neq m'}(U_{mm'} - J_{mm'})\, f^{\dagger}_{m,\sigma} f_{m,\sigma} f^{\dagger}_{m',\sigma} f_{m',\sigma} + \sum_{m,m'} U_{mm'} f^{\dagger}_{m,\uparrow} f_{m,\uparrow} f^{\dagger}_{m',\downarrow} f_{m',\downarrow} \tag{9}$$

which can be decomposed at the mean-field level into

$$H_U = \sum_{m,\sigma} f^\dagger_{m,\sigma} f_{m,\sigma} \left[\sum_{m'} U_{mm'} n_{m',-\sigma} + \sum_{m' \neq m} (U_{mm'} - J_{mm'}) n_{m,'\sigma} \right], \text{ where}$$

$$n_{m,\sigma} = \langle f^\dagger_{m,\sigma} f_{m,\sigma} \rangle \tag{10}$$

is the occupation of the orbital with angular momentum projection m and spin σ. The summation is carried over the degenerate orbitals in a given irredubile representation, which in graphene correspond to the doublets $m = \pm |l_z|$, with $|l_z| = 0, 1, \ldots, l$. The mean field interaction can be absorbed into the definition of the localized energy level in equation (4),

$$H_f = \sum_{\sigma,m} \epsilon_{m,\sigma} \, f^\dagger_{m,\sigma} f_{m,\sigma} \, , \tag{11}$$

where

$$\epsilon_{m,\sigma} \equiv \epsilon_0 + \sum_{m'} U_{mm'} n_{m',-\sigma} + \sum_{m' \neq m} (U_{mm'} - J_{mm'}) n_{m,'\sigma}$$

is the spin dependent renormalized energy of the localized states in a given irreducible representation.

3. Local magnetic moments

The formation of local magnetic moments can be addressed by the self-consistent calculation of the occupation for up and down spin states in the different orbitals, which follows from integrating the DOS from the bottom of the band up to the Fermi level μ [5, 31]:

$$n_{m,\sigma} = -\frac{1}{\pi} \int_{-\infty}^{\mu} \mathrm{d}\omega \, \mathrm{Im} \, G^{\mathrm{R}}_{ff,m,\sigma}(\omega), \tag{12}$$

where

$$G^{\mathrm{R}}_{ff,m,\sigma}(\omega) = \left[\omega - \epsilon_{m,\sigma} - \Sigma_{ff,m}(\omega) + \mathrm{i}0^+ \right]^{-1} \tag{13}$$

is the retarded Green's function of the localized electrons, $G_{ff,\sigma}(\tau) = -\langle T[f(\tau) f^\dagger(0)\rangle$, and

$$\Sigma_{ff,m}(\omega) = \sum_{x,y} \sum_{\mathbf{p}} \left[V^{(m)}_{x,\mathbf{p}} \right]^* G^{0\,\mathrm{R}}_{xy}(\mathbf{p}, \omega) V^{(m)}_{y,\mathbf{p}} \tag{14}$$

is the self-energy of the f-electrons, with $x = a, b$. $\hat{G}^{0\,\mathrm{R}}_{x,y}$ are the matrix elements of the retarded Green's function of the itinerant electrons in graphene, $G^0_{aa,\mathbf{p}}(\tau) = -\langle T[a_{\mathbf{p}}(\tau) a^\dagger_{\mathbf{p}}(0)]\rangle$ and so on, which are defined by

$$\hat{G}(\mathbf{p}, \mathrm{i}\omega) = \frac{1}{\mathrm{i}\omega - \hat{H}} \, , \tag{15}$$

where

$$\hat{H} = -t \begin{pmatrix} 0 & \phi_{\mathbf{p}} \\ \phi^*_{\mathbf{p}} & 0 \end{pmatrix} \tag{16}$$

is the tight-binding Hamiltonian matrix. More explicitly,

$$G^{0,\mathrm{R}}_{xy}(\mathbf{p},\omega)=\frac{1}{2}\sum_{\alpha=\pm}\frac{\mathbf{1}+\alpha\hat{\sigma}_{xy,\mathbf{p}}}{\omega-t\alpha|\phi_{\mathbf{p}}|+\mathrm{i}0^{+}}, \tag{17}$$

where

$$\hat{\sigma}_{xy,\mathbf{p}}\equiv\frac{\mathrm{Re}(\phi_{\mathbf{p}})\sigma^{1}_{xy}-\mathrm{Im}(\phi_{\mathbf{p}})\sigma^{2}_{xy}}{|\phi_{\mathbf{p}}|}\,, \tag{18}$$

1 is the identity matrix and σ^{1} and σ^{2} are off-diagonal 2×2 Pauli matrices, namely $\sigma^{1}_{ab}=\sigma^{1}_{ba}=1$ and $\sigma^{2}_{ab}=-\sigma^{2}_{ba}=-\mathrm{i}$.

The Green's function of the localized electrons can be written more explicitly in the following form:

$$G^{\mathrm{R}}_{ff,m,\sigma}(\omega)=\frac{1}{\omega Z^{-1}_{m}(\omega)-\epsilon_{m,\sigma}+\mathrm{i}\Delta^{(m)}(\omega)+\mathrm{i}0^{+}}\,, \tag{19}$$

where

$$Z^{-1}_{m}(\omega)=1-\frac{1}{\omega}\mathrm{Re}\;\Sigma_{ff,m}(\omega) \tag{20}$$

gives the quasi-particle residue and $\Delta(\omega)\equiv-\mathrm{Im}\;\Sigma_{ff}(\omega)$ is the level broadening of the localized state [25]

$$\Delta^{(m)}(\omega)=\left[V^{(m)}\right]^{2}\sum_{\mathbf{p},\alpha}|\Theta^{(m)}_{\alpha,\mathbf{p}}|^{2}\delta(\omega-\alpha|\phi_{\mathbf{p}}|) \tag{21}$$

which is defined in terms of the generic tight-binding phases

$$\Theta^{(m)}_{\alpha,\mathbf{p}}\equiv\frac{1}{\sqrt{2}V^{(m)}}\left(V^{(m)}_{b,\mathbf{p}}+\alpha\frac{\phi^{*}_{\mathbf{p}}}{|\phi_{\mathbf{p}}|}V^{(m)}_{a,\mathbf{p}}\right), \tag{22}$$

where $V^{(m)}\equiv\max(V^{(m)}_{x,i})$.

Those phases depend explicitly on the symmetry of the localized orbital, which reflect in the relative amplitudes of hybridization with the surrounding carbon atoms, and also on the relative position of the adatom with respect to the sublattices, i.e if the adatom sits on top of a carbon, in the center of the honeycomb hexagon, on a bridge site or else in a substitutional site. This formulation is completely general and can be easily extended to include for instance substitutional impurities in double vacancies.

In the scenario where the adatom sits on top of a carbon atom, the level broadening is given by $\Delta(\omega)=\pi V^{2}\rho(\omega)$, where $\rho(\omega)=|\omega|/D^{2}$ is the DOS in graphene in the linear portion of the spectrum, and therefore $\Delta(\omega)$ scales linearly with energy. For adatoms that sit on H or S sites, the scaling analysis of the level broadening allows a classification in two symmetry groups, depending on either if the $C_{3\mathrm{v}}$ point group symmetry of the honeycomb sublattice is preserved by the adatom or not, as previously mentioned in the introduction. As illustrated in figure 3, when the electrons hop in and out of an adatom sitting on H or S sites, they collect phases which give rise to quantum mechanical interference among the possible hybridization paths. When the amplitudes of hybridization of a localized orbital with the three surrounding carbons on the same sublattice are identical, in which case the $C_{3\mathrm{v}}$ point group symmetry of sublattice x is preserved, the hopping phases interfere and give rise to an anomalous energy scaling of the

hybridization, whose modulus scales now in the same way as the kinetic energy, $|V_{x,\mathbf{p}}| \propto |\phi_{\mathbf{p}}|$. In that case, the level broadening scales as [22, 25]

$$\Delta^{(m)}(\omega) \approx \pi [V^{(m)}]^2 \rho(\omega) \frac{|\omega|^2}{t^2} \tag{23}$$

at low energy, as opposite to the conventional case where this interference is frustrated and $|V_{x,\mathbf{p}}|$ scales to a constant near the Dirac points. In the latter, $\Delta(\omega) \propto \rho(\omega)$ corresponds to the standard case, whereas in the former case the damping is super-linear. The first class of orbitals, which we will refer as type II orbitals, include $m = 0$ and 3 angular momentum states, such as in s and in-plane f-wave orbitals. The standard 'ohmic' class (type I) by its turn is described by adatoms on top carbon sites and $m = \pm 1$ and ± 2 angular momentum orbitals on H or S sites. To be more concrete, the class of type I orbitals is represented by adatoms that sit on top of a carbon atom, in which case the orbital symmetry is not particularly important, and also by adatoms siting at H or S sites with localized orbitals in the $E_1(\mathrm{d}_{xz},\mathrm{d}_{yz})$ (i.e. $m = \pm 1$) and $E_2(\mathrm{d}_{xy}, \mathrm{d}_{x^2-y^2})$ ($m = \pm 2$) representations of d-wave orbitals and also f_{xz^2}, f_{yz^2}, f_{xyz}, $\mathrm{f}_{z(x^2-y^2)}$ orbitals in H/S sites. The class of type II orbitals is described by s, d_{zz}, f_{z^3} orbitals, where $m = 0$, and also by $\mathrm{f}_{x(x^2-3y^2)}$ and $\mathrm{f}_{y(3x^2-y^2)}$ orbitals ($m = \pm 3$) in H or S sites. The anomalous scaling of the level broadening in equation (23) has been verified explicitly by *ab initio* methods, in particular for the d_{zz} orbital of Co on graphene [33].

The self-energy of the localized electrons (see equation (14)) can be more explicitly written in the form

$$\Sigma_{ff,m}(\omega) = -\omega \left[Z_m^{-1}(\omega) - 1 \right] - \mathrm{i}\Delta^{(m)}(\omega) |\theta(D - |\omega|) \tag{24}$$

The density of states of the localized level, $\rho_{ff,m,\sigma}(\omega) = -1/\pi \,\mathrm{Im}\, G^{\mathrm{R}}_{ff,m,\sigma}(\omega)$ follows from the substitution of equation (24) into (13):

$$\rho_{ff,m,\sigma}(\omega) = \frac{1}{\pi} \frac{\Delta^{(m)}(\omega)\theta(D - |\omega|)}{[\omega Z_m^{-1}(\omega) \ - \epsilon_{m,\sigma}]^2 + \left[\Delta^{(m)}(\omega)\right]^2} \tag{25}$$

In the linear cone approximation, where the spectrum is linearized around the Dirac points, $t|\phi_{\mathbf{K}+\mathbf{p}}| \to vp$ up to the cut-off of the band D, with $v \approx 6\,\mathrm{eV\AA}$ as the Fermi velocity, the level broadening for orbitals of type I is

$$\Delta_I(\omega) \equiv \Delta_0 |\omega| \tag{26}$$

at low energies, where $\Delta_0 = \pi (V/D)^2$ is the dimensionless hybridization parameter, and

$$Z^{-1}_{\mathrm{I},m}(\omega) = (\Delta_0^{(m)}/\pi) \ln \left| 1 - D^2/\omega^2 \right| \tag{27}$$

implying that the quasi-particle residue $Z \to 0$ vanishes logarithmically at low energy.

In the case of super-linear damping, for type II orbitals, the level broadening scales with the *cube* of the energy within the linear cone approximation,

$$\Delta_{\mathrm{II}}(\omega) = N_{\mathrm{s}} \Delta_0 |\omega|^3 / t^2 \tag{28}$$

and can be orders of magnitude smaller than in the linear case when $|\epsilon_0| \ll t$. $N_{\mathrm{s}} = 1, 2$ correspond to the number of sublattices the adatom effectively hybridizes ($N_{\mathrm{s}} = 2$ for H

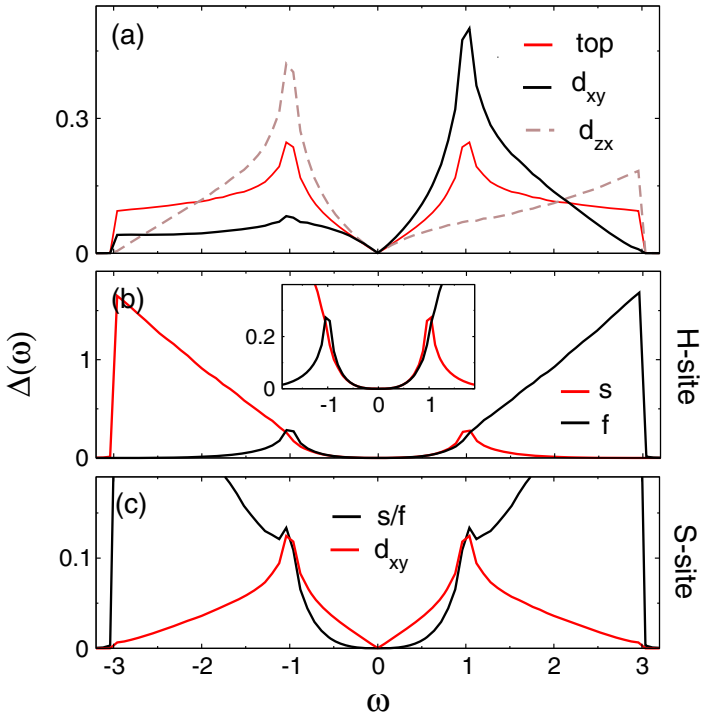

Figure 4. Level broadening $\Delta(\omega)$ as a function of energy, ω, for different orbital symmetries. All energies in units of the hopping energy t ($V/t = 1/3$). (a) Type I orbitals for adatoms sitting on a top carbon site (red solid curve) and for d_{xy}-wave (black line) and d_{zx}-wave orbitals (dashed line) on H sites. (b) Type II orbitals on H sites. Black curve: in-plane f-wave orbital; red curve: s-wave orbital. Inset: low energy scaling of the level broadening, $\Delta(\omega) \propto |\omega|^3$ for $|\omega|/t < 1$ (see text). (c) Substitutional s/f-wave orbitals (black curve) and d_{xy}-wave orbital (red curve), on S sites.

sites and $N_s = 1$ for S sites, as shown in figure 3). The quasi-particle residue, Z_σ, in this approximation is given by

$$Z^{-1}_{\mathrm{II},m}(\omega) = 1 + \frac{N_s \Delta_0^{(m)}}{\pi t^2}\left[D^2 + \omega^2 \ln|1 - D^2/\omega^2|\right]. \tag{29}$$

In all cases, the level broadening can be severely affected in the presence of out-of-plane magnetic fields, which produce Landau level quantization and nonlinear orbital magnetization effects in graphene [32].

In figure 4, we show the energy scaling of the level broadening for the different orbital symmetries. Particle–hole symmetry is preserved for adatoms on top carbon sites, where $\Delta(\omega)$ follows the DOS, and also for adatoms on S sites, which effectively hybridize with only one sublattice. For adatoms on H sites, which hybridize with the two sublattices, particle–hole symmetry is explicitly broken in the high energy sector ($|\omega| \gtrsim t$) by the off diagonal matrix elements of the hybridization (at low energy, the off diagonal terms average to zero in the momentum integrals). In particular, $d_{x^2-y^2}$, d_{xy}-wave orbitals (where $V_{a,i} = V_{b,i}$) are strongly damped when the energy of the localized state is far above the Dirac point ($\omega > t$), but otherwise are weakly damped at negative energy states (black solid curve in figure 4(a)). Conversely, d_{zx} and d_{zy}-wave orbitals (where $V_{a,i} = -V_{b,i}$) show the opposite trend, in agreement with

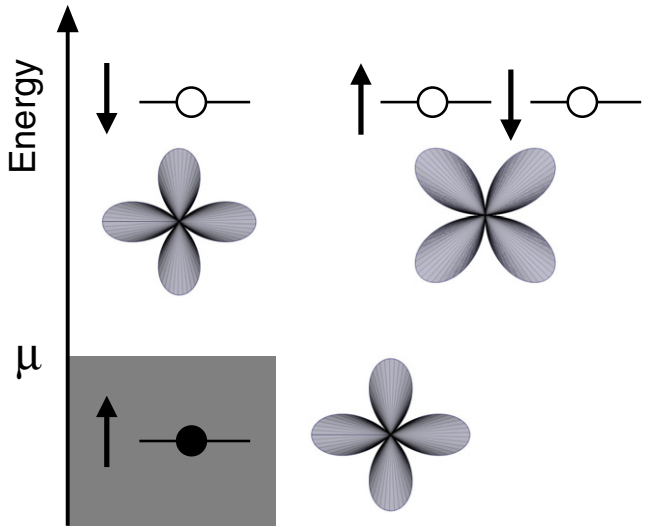

Figure 5. Maximal spin and orbital polarization for degenerate doublet states, say $d_{x^2-y^2}$ and d_{xy} ($m = \pm 2$). When the bare levels are occupied $\mu - \epsilon_0 > 0$ and the virtual doubly occupied state is empty, $\epsilon_0 + U \gg \mu$, where U is the Coulomb energy, the energy of the doublet state is maximally polarized in the regime where $U \gg J,\ \Delta$, where J is the exchange energy and Δ is the level broadening due to the hybridization with the bath. In this limit, the spin and orbital polarized levels have occupation $n_{m,\sigma} \sim 1$, and $n_{m,-\sigma} = n_{-m,\sigma} = n_{-m,-\sigma} \sim 0$ (spin $1/2$) (see [27]) with $\sigma = \uparrow\downarrow$.

ab initio calculations for Co adatoms in graphene [33, 34]. In the same way, s and in-plane f-wave orbitals, which couple symmetrically and anti-symmetrically with the two sublattices respectively, show a strong particle–hole asymmetry at high energies, as depicted in figure 4(b). In figure 4(c), we show the level broadening for the substitutional case, where particle-hole symmetry is restored. In all cases, the peaks at $|\omega| = t$ are divergences which are reminiscent of the logarithmic singularity of the DOS around the M point of the Brillouin zone (BZ).

3.1. Single orbital picture: the case of spin $1/2$ *adatoms*

The arguments outlined so far are completely general, and apply to any adatom in graphene containing localized electronic states. Now, for convenience and simplicity, we will restrict our analysis to adatoms that can be described by an effective single orbital picture.

Let us consider for instance two degenerate orbitals contained in a given irreducible representation of the honeycomb lattice, say d_{xy} and $d_{x^2-y^2}$, with $m = \pm 2$. We assume that the bare degenerate energy levels are occupied, $\epsilon_0 - \mu < 0$, and the virtual doubly occupied states are empty, $\epsilon_0 + U \gg \mu$. In the situation where Coulomb repulsion in the orbitals U is much larger that the exchange coupling J and the level broadening Δ due to the hybridization of the orbitals, namely $U \gg J,\ \Delta$, the lowest energy solution for a doublet is a maximally polarized state where one orbital is fully spin polarized (say $d_{x^2-y^2}$) and the other is empty (hence with total spin $1/2$ and total charge of one electron) [27], as illustrated in figure 5. In this regime, where only one orbital of the doublet is occupied, the energy separation between the orbitals is set by the Coulomb interaction, U, which is typically of the order of a few eV. The spin and the charge of the polarized orbitals will fluctuate among four minima, which describe the four

possible degenerate configurations with the lowest energy, namely

$$n_{m,\sigma} \sim 1, \quad n_{m,-\sigma} = n_{-m,\sigma} = n_{-m,-\sigma} \sim 0 \tag{30}$$

for $m = \pm|m|$ and $\sigma = \uparrow, \downarrow$. The orbital degeneracy of the four minima can be lifted through a Jahn–Teller effect distortion created by local lattice deformations.

In real crystals, the adatoms are known to locally deform the lattice, and those deformations extend over several lattice sites [26]. In the situation where the adatoms are randomly distributed, those distortions will displace the adatoms from the high symmetry positions and create crystalline field anisotropies. Those anisotropies will select one of the two degenerate orbitals and 'freeze' their occupation at energy scales smaller that the crystalline field anisotropy energy. When this criterion is fulfilled and $U \gg J,\ \Delta$, the electronic transitions between the orbitals are suppressed and the effective Hamiltonian of the spin polarized orbital can be approximated for all purposes by the Hamiltonian of the *single* orbital problem, up to small corrections due to the direct Coulomb interaction between the orbitals. We will assume the local deformations in graphene to be small but enough to lift the orbital degeneracies of the adatoms beyond the experimental STM energy resolution.

The single orbital problem was described in the original work by Anderson [31]. The Coulomb Hamiltonian of the spin polarized orbital is approximately described by

$$H_U = U\ f_\uparrow^\dagger f_\uparrow f_\downarrow^\dagger f_\downarrow \tag{31}$$

and orbital indexes (m) are suppressed everywhere else in Hamiltonian (1). The energy of the localized orbital becomes

$$H_f = \sum_\sigma \epsilon_\sigma\ f_\sigma^\dagger f_\sigma \tag{32}$$

where $\epsilon_\sigma = \epsilon_0 + U n_{-\sigma}$ gives the energy of the spin polarized level.

In the single orbital problem, as in the degenerate case, the occupation for up and down spin states can be self-consistently calculated at the mean field level from equation (12). The emergence of a local magnetic moment follows from the appearance of a spin polarized state below the Fermi level, say, at energy $\epsilon_0 + n_\uparrow U$, and a virtual (empty) state at $\epsilon_0 + n_\downarrow U$ for the majority spin, with $n_\uparrow + n_\downarrow \leqslant 2$ due to the Pauli principle.

The analysis about the formation of local magnetic moments and the zero-dimensional phase diagram that comes out of the single orbital picture has been discussed in detail in [5] for the case of type I orbitals. For type II orbitals, the physics is qualitatively similar, except for the fact that the formation of a local magnetic moment becomes exceedingly easy, even at small U, due to the fact that the broadening of the level can be negligibly small when $\epsilon_0/t \ll 1$.

From now on, we will drop the orbital indices m and consider only spin polarization effects on a given orbital.

4. Local density of states

The LDOS around the impurity can be computed directly from the diagonal matrix elements of the electronic Green's function in graphene in the presence of the adatom,

$$\rho_x(\mathbf{r}, \omega) = -\frac{1}{\pi}\mathrm{Im} \sum_\sigma \sum_{\mathbf{p},\mathbf{p}'} G^{\mathrm{R}}_{xx,\sigma}(\mathbf{p}, \mathbf{p}', \omega)\, \mathrm{e}^{\mathrm{i}(\mathbf{p}-\mathbf{p}')\mathbf{R}}, \tag{33}$$

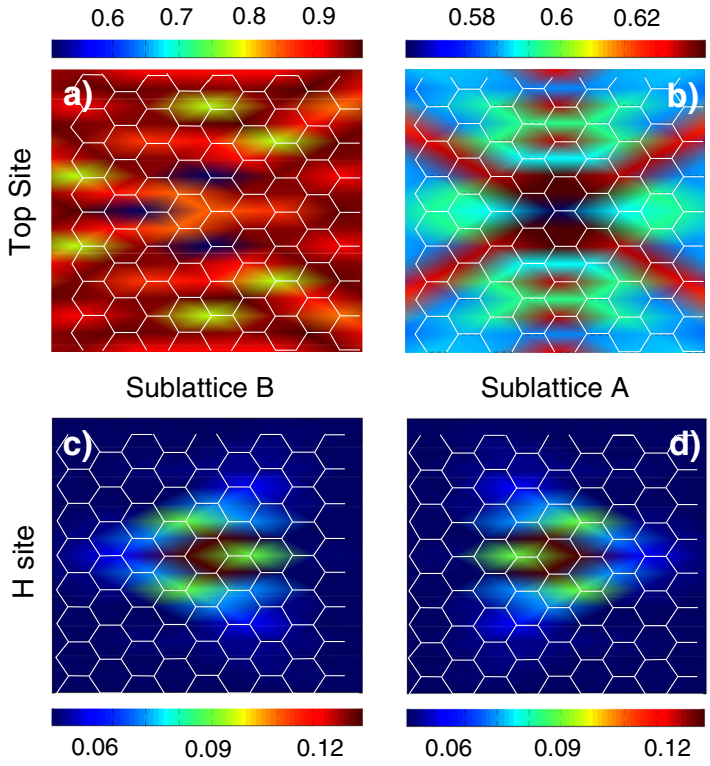

Figure 6. Comparison of the LDOS between the two different sublattices. Top panels: energy integrated LDOS around an adatom (center) sitting on a top carbon adatom site. Scans for (a) the opposite sublattice of the impurity and (b) for the same sublattice. Lower panels: energy integrated LDOS around a localized orbital (center) with s-wave symmetry, when the adatom sits in the center of a honeycomb hexagon (H site). (c) scans for sublattice A and (d) B. The two scans are related by a π-rotation.

where

$$G_{xy,\sigma}(\mathbf{p},\mathbf{p}',\mathrm{i}\omega) = \delta_{\mathbf{p},\mathbf{p}'}G^0_{xy}(p) + \Lambda_x(p)G_{ff,\sigma}(\mathrm{i}\omega)\bar{\Lambda}_y(p') \tag{34}$$

and

$$\Lambda_x(p) \equiv \sum_{y=a,b} G^0_{xy}(p)V_{y,\mathbf{p}}, \tag{35}$$

$$\bar{\Lambda}_x(p) \equiv \sum_{y=a,b} V^*_{y,\mathbf{p}}G^0_{yx}(p) \tag{36}$$

with $V_{a,\mathbf{p}}$ and $V_{b,\mathbf{p}}$ defined in equations (7) and (8).

In figure 6 we show the topography maps around the impurity, which describe the LDOS integrated in energy. We use the set of parameters $V = 1\,\mathrm{eV}$, $U = 1\,\mathrm{eV}$, $\mu = 0.1\,\mathrm{eV}$ and $\epsilon_0 = -0.5\,\mathrm{eV}$. Those energy scales describe the typical order of magnitude for the charging energy U and the hybridization V of transition metals in graphene [24]. In the case where the adatoms sit on top of a carbon site on a given sublattice (top panels), the maps show a clear asymmetry between the integrated LDOS of the two different sublattices. The pattern on the opposite sublattice of the impurity (figure 6(a)) has a lower point group symmetry than in the same sublattice (figure 6(b)), what comes from the fact that the adatom in this case has only

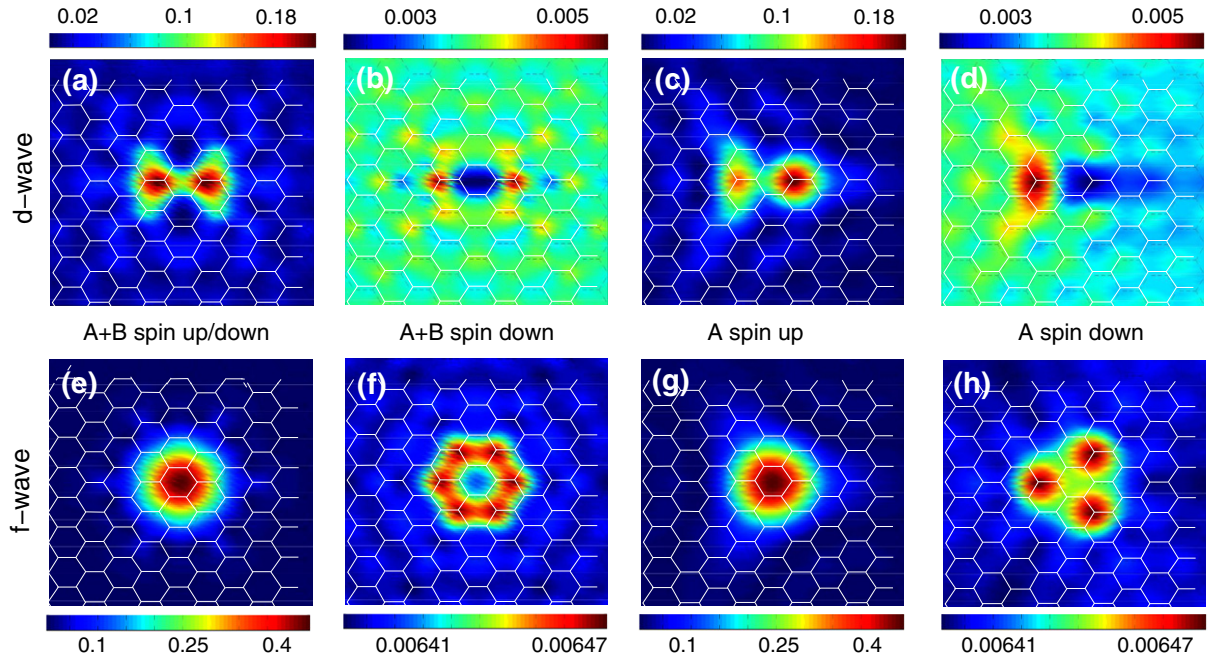

Figure 7. LDOS around the adatom (center) at a fixed energy ($\omega = -0.2\,\mathrm{eV}$) for adatoms on H sites. The top row corresponds to a $d_{x^2-y^2}$ orbital and the bottom row to an in-plane f-wave orbital. (a), (e) Total LDOS; (b), (f) LDOS for the minority spin; (c), (g) LDOS for the majority spin on sublattice A and (d), (h) LDOS for the minority spin on sublattice A.

three nearest-neighbor carbon sites but six next-nearest-neighbor ones. For adatoms sitting in the center of the honeycomb hexagon (lower panels), there is no distinction between the patterns of the two different sublattices, except for a rotation of π. Figures 6(c) and (d) depict the integrated LDOS for an s-wave orbital ($m = 0$) sitting on an H site. The intensity of the integrated LDOS maps is also much weaker in the lower panels compared to the upper ones, reflecting the fact that the hybridization for H or S sites is mediated by hopping, and hence weaker than in the top carbon site case for the same set of parameters. Only recently STM experiments observed the topography around isolated Fe and Co adatoms in graphene [35]. X-ray magnetic circular dichroism experiments revealed that these adatoms have a large local magnetic moment [35].

The analysis of the LDOS also permits to identify the symmetry of the localized orbital when the adatom sits either on H or S sites. In figure 7 we show the LDOS at fixed energy for both a $d_{x^2-y^2}$ orbital (figures 7(a)–(d)) and a $f_{x(x^2-3y^2)}$ state (figure 7(e)–(h)). In the former, the orbital d-wave symmetry of the localized state has a clear fingerprint in the induced DOS nearby the adatom. The signature is specially pronounced when the LDOS is resolved for the minority spins, as noticed by direct comparison of figures 7(b) and (f). In panels (c), (d) and (g), (h), we show the distinct patterns for the LDOS of majority and minority spins on a given sublattice. In the case of an in-plane f-wave state, which explicitly preserves the point group symmetry of the sublattices, the fingerprint, although more subtle, can be easily characterized by a Fourier analysis of the LDOS, which maps the scattering wavevectors responsible for the emergence of local resonances nearby the adatom.

In figure 8, we plot the corresponding maps of the energy integrated LDOS in the reciprocal space. The solid hexagonal line indicates the BZ. In figure 8(a), we show the maps for the

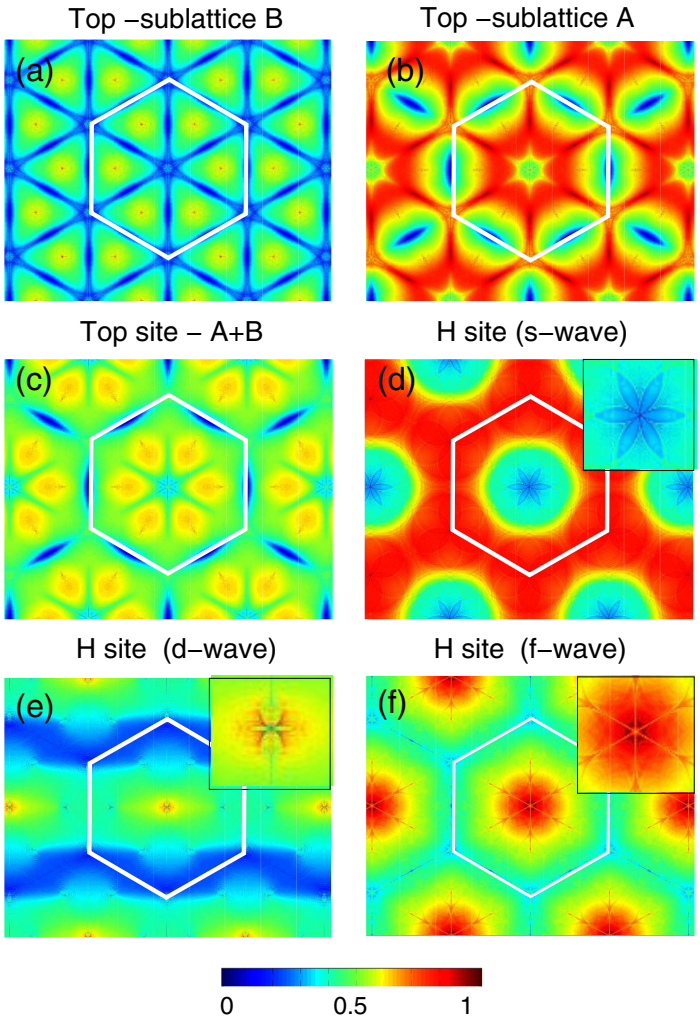

Figure 8. Fourier transform of the energy integrated LDOS around a spin 1/2 adatom. Solid hexagon line indicates the BZ. The peaks at the center of the zone correspond to forward scattering processes, whereas the peaks at the corners of the zone (K) points correspond to backscattering between the two valleys. Top panels: adatom on a top carbon site case; Fourier transform of the LDOS for the (a) opposite and (b) same sublattice of the adatom. (c) Superposition of the patterns in panels (a) and (b), for both sublattices. (d) s-wave orbital at an H site. Lower panels: (e) $d_{x^2-y^2}$-wave orbital and (f) $f_{x(x^2-3y^2)}$ orbital also at H sites. The insets in panels (d)–(f) show the details of the forward scattering peaks at the center of the BZ.

opposite sublattice of the impurity, whereas on figure 8(b), we depict the Fourier transformed maps for the same sublattice of the adatom. The central peaks around the center of the zone (Γ point) indicate forward scattering processes that contribute to the resonant states near the adatom, whereas the peaks centered at the K points at the edges the BZ indicate backscattering processes, which connect the different valleys. For the opposite sublattice of the adatom (figure 8(a)), the backscattering processes at the K point and the forward scattering ones at Γ are significantly attenuated. In the reciprocal space maps for the *same* sublattice of the impurity (figure 8(b)), where unitary scattering should dominate, backscattering processes are strongly

enhanced, followed by the presence of subdominant forward scattering peaks. In panel 8(c), we depict the Fourier transformed map for both sublattices. In those plots (top carbon case), the amount of scattering at the M points, which indicate the position of the Van Hove singularities, is weak compared to the other dominant processes. The shape of the forward scattering peak at the Γ point also reflects the symmetry of the hybridization matrix elements in the Hamiltonian. In the top carbon case, the Γ peak is isotropic.

In figure 8(d) we show the reciprocal space maps for the energy integrated LDOS for an s-wave orbital siting at an H site. In this case, the height of the central peak is significantly small compared to the dominant peaks around the K points, indicating strong enhancement of the backscattering compared to forward scattering processes. In panel 8(e) we depict the case of a $d_{x^2-y^2}$-wave orbital also at an H site, whereas in panel 8(f) we show the signature of an $f_{x(x^2-3y^2)}$ orbital (H site) in the reciprocal space. For d and f-wave orbitals, destructive interference leads to attenuation of the backscattering peaks at the K points, in particular in the d-wave case. In the insets of figures 8(d) and (f) we show in detail the features of the forward scattering peaks for s-wave and $f_{x(x^2-3y^2)}$-wave orbitals, respectively. Both peaks reflect the underlying C_{3v} symmetry of the sublattices, which are incorporated into the hybridization matrix elements of the Hamiltonian for orbitals of type II. For a d-wave orbital (inset of figure 8(e)), the forward scattering peak has C_{2v} symmetry.

5. STM tip effects

Let us now consider a problem of more practical interest for tunneling microscopy experiments, where we include an STM tip close to a spin 1/2 impurity. The electrons in the metallic tip follow the Hamiltonian

$$H_t = \sum_{\mathbf{p}} \epsilon_{\mathbf{p}} c^{\dagger}_{\sigma \mathbf{p}} c_{\sigma \mathbf{p}}, \tag{37}$$

where $\epsilon_{\mathbf{p}} = p^2/2m$ is the electronic dispersion of an electron gas, with m the effective mass. The electrons can tunnel either to the carbon sites in graphene or to the impurity. In the former case, the tunneling process is described by the Hamiltonian

$$H_{g-t} = \sum_{\langle i \rangle} \sum_{\sigma} t_a a^{\dagger}_{\sigma}(\mathbf{R}_i) c_{\sigma}(\mathbf{R}_i - \mathbf{r}) + \sum_{\langle i \rangle} \sum_{\sigma} t_b b^{\dagger}_{\sigma}(\mathbf{R}_i) c_{\sigma}(\mathbf{R}_i - \mathbf{r}) + \text{h.c.}, \tag{38}$$

where t_a, t_b are the electronic tunneling energy from the tip to sublattices A and B in graphene, $\langle i \rangle_t$ denotes the sum over the tip nearest-neighbor carbon sites ($\mathbf{R}_i$) on a given sublattice, and $\mathbf{r} = (R, z)$ is the position of the center of the tip, where $\mathbf{R}$ is the horizontal distance of the tip to the impurity and z is the distance of the tip to the graphene layer (see figure 9).

The single-particle wave-functions $\psi_{t,\mathbf{p}}(\mathbf{r})$ describing the electronic state at the tip, namely

$$c_{\sigma}(\mathbf{R}_i - \mathbf{r}) = \sum_{\mathbf{p}} \psi_{t,\mathbf{p}}(\mathbf{R}_i - \mathbf{r}) c_{\sigma \mathbf{p}}$$

can be expanded in spherical waves from the center of the tip, $\psi_{t,\mathbf{p}}(r) \propto e^{-\kappa_{\mathbf{p}} r}/r$, where $c_{\sigma \mathbf{p}}$ is a second quantized operator for the tip electrons. The factor [19, 20]

$$\kappa_{\mathbf{p}} = \sqrt{2m(\phi_t - \epsilon_{\mathbf{p}})} \tag{39}$$

gives the effective tunneling barrier between the tip and the rest of the system, and is defined by the electronic work function of the tip, ϕ_t. Since the single-particle wave functions of the

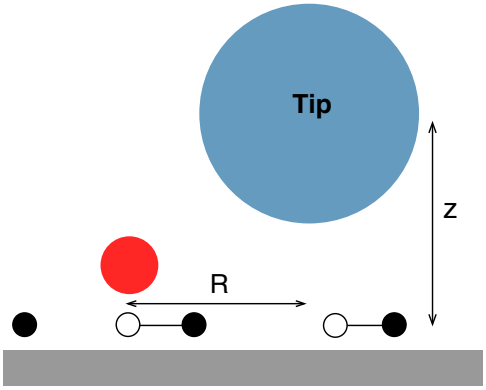

Figure 9. Schematic drawing of the STM tip nearby an adatom (small light (red) circle) on top of graphene. Black and white circles: carbon atoms on sublattices A and B. R is the in-plane distance of the impurity to the tip and z the out-of-plane distance from the center of the tip to the graphene layer.

graphene electrons can be expanded in plane waves, $\psi_{g,\mathbf{k}}(\mathbf{R}_i) = e^{i\mathbf{k}\mathbf{R}_i}$ [19], the Hamiltonian (38) becomes

$$H_{g-t} = \sum_{\sigma} \sum_{\mathbf{kp}} \left[t_{a,\mathbf{kp}}(\mathbf{r})\, a^{\dagger}_{\sigma\mathbf{k}} c_{\sigma\mathbf{p}} + t_{b,\mathbf{kp}}(\mathbf{r})\, b^{\dagger}_{\sigma\mathbf{k}} c_{\sigma\mathbf{p}} \right] + \text{h.c.}, \tag{40}$$

where

$$t_{x,\mathbf{kp}}(\mathbf{r}) \sim \frac{t_x}{z} \mathrm{e}^{-\kappa_{\mathbf{p}} z} \mathrm{e}^{-i\mathbf{k}\mathbf{R}} \equiv t_{x,\mathbf{p}}(z)\, \mathrm{e}^{-i\mathbf{k}\mathbf{R}} \tag{41}$$

describes the spatially averaged hopping matrix elements between the tip and graphene, where the position of each of the carbon atoms underneath the tip is effectively replaced by the in-plane position of the center of the tip with respect to the impurity.

The Hamiltonian for the tunneling from the tip to the impurity is given by

$$H_{f-t} = t_f \sum_{\sigma} f^{\dagger}_{\sigma} c_{\sigma}(\mathbf{r}) + \text{h.c.}, \tag{42}$$

where t_{f-t} is the tunneling energy from the tip to the impurity. In a similar way, we can write

$$H_{f-t} = \sum_{\sigma,\mathbf{p}} t_{f,\mathbf{p}}(r) f^{\dagger}_{\sigma} c_{\sigma\mathbf{p}} + \text{h.c.}, \tag{43}$$

where

$$t_{f,\mathbf{p}}(r) = t_f \frac{1}{|\mathbf{r}|} \mathrm{e}^{-\kappa_{\mathbf{p}}|\mathbf{r}|}, \tag{44}$$

where $|\mathbf{r}| = \sqrt{R^2 + z^2}$ measures the center of the tip with respect to the position of the impurity. We will assume that the tip is sufficiently large such that local gating effects due to the proximity of the tip to graphene can be effectively absorbed into the local definition of the chemical potential nearby the adatom [18].

As a brief comment about orders of magnitude for the several quantities, in most materials, the typical work function ϕ_t is of the order of a few eV. In the case where the effective mass m is of the same order of the bare mass of the electron, $\kappa_{\mathbf{p}}^{-1}$, translates into a characteristic tunneling length scale topically larger than 1 nm. Also, since STM tips have a typical radius of the order

of 1 nm, z, which accounts for the distance between the center of the tip to graphene is typically a number of the same order. A more detailed description about the characterization of the tip and the surface in the STM problem can be found in [19].

5.1. Green's functions

Now we generalize the original Hamiltonian of the Anderson problem to include Hamiltonian terms (37), (40) and (43),

$$H = H_g + H_f + H_V + H_U + H_t + H_{g-t} + H_{f-t} \tag{45}$$

In the following, we will assume perturbation theory in the hybridization of the tip with the rest of the system, namely t_f and t_x ($x = a,\ b$) are small compared to the hybridization V of the adatom with the host (graphene). This is not nevertheless a strict requirement at the mean field level, and the 'exact' expressions of the Green's functions are shown in the appendix. In addition, we will also assume that the system remains in equilibrium in the presence of the STM tip. A detailed calculation of the equilibrium and also out of equilibrium Green's functions in the STM problem for metallic surfaces can be found in [20].

To further simplify matters, we assume here that $\kappa_{\mathbf{p}} \sim \kappa$ is computed at the Fermi energy and hence is momentum independent, in which case

$$t_{x,\mathbf{kp}}(\mathbf{r}) \to t_x(z)\, \mathrm{e}^{-\mathrm{i}\mathbf{kR}} \equiv t_{x,\mathbf{k}}(\mathbf{r}) \tag{46}$$

with $x = a,\ b$. Since the STM tip is typically large compared to the lattice spacing in graphene, one can further simplify things by assuming $t_{a,\mathbf{p}} = t_{b,\mathbf{p}}$. We will keep the $a,\ b$ labels below for completeness. A similar assumption will be made for the tunneling matrix element between the tip and the adatom, $t_{f,\mathbf{p}}(r) \to t_f(r)$.

The matrix elements of the renormalized Green's function is the $a,\ b$ sublattice basis can be calculated straightforwardly,

$$\begin{aligned} G_{xy,\sigma}(\mathbf{p}, \mathbf{p}', \mathrm{i}\omega) &= \delta_{\mathbf{p},\mathbf{p}'} G^0_{xy}(p) + \Gamma_x(p, \mathbf{r})\Lambda_x(p) G_{ff,\sigma}(\mathrm{i}\omega)\bar{\Lambda}_y(p')\bar{\Gamma}_y(p', \mathbf{r}) \\ &+ T_x(p, \mathbf{r})\bar{T}_y(p', \mathbf{r}) \sum_{\mathbf{k}} G^0_{cc}(k). \end{aligned} \tag{47}$$

The quantities $\Lambda_x(p)$ and $\bar{\Lambda}_x(p)$ were defined in equations (35) and (36), whereas

$$T_x(p, \mathbf{r}) \equiv \sum_{y=a,b} G^0_{xy}(p) t_{y,\mathbf{p}}(\mathbf{r}), \tag{48}$$

$$\bar{T}_x(p, \mathbf{r}) \equiv \sum_{y=a,b} t^*_{y,\mathbf{p}}(\mathbf{r}) G^0_{yx}(p) \tag{49}$$

contain the tunneling amplitudes and phases for the electrons as they hop between the tip and the A and B sublattices. $G^0_{cc}(\mathbf{k}, \tau) = -\langle T[c_{\mathbf{k}}(\tau)c^{\dagger}_{\mathbf{k}}(0)]\rangle$ is the bare Green's function of the electrons of the tip,

$$G^0_{cc}(p) = \frac{1}{\mathrm{i}\omega - \epsilon_{\mathbf{p}}} \tag{50}$$

while Γ and its conjugate form $\bar{\Gamma}$ in equation (47) define the vertex renormalization due to the presence of the tip,

$$\Gamma_x(p, \mathbf{r}) = 1 + \frac{T_x(p, \mathbf{r})}{\Lambda_x(p)} \bar{t}_f(\mathbf{r}, \omega) \sum_{\mathbf{k}} G^0_{cc}(k), \tag{51}$$

$$\bar{\Gamma}_x(p,\mathbf{r}) = 1 + \frac{\bar{T}_x(p,\mathbf{r})}{\bar{\Lambda}_x(p)} t_f(\mathbf{r},\omega) \sum_{\mathbf{k}} G^0_{cc}(k), \tag{52}$$

where the quantities

$$t_f(\mathbf{r},\mathrm{i}\omega) = t_f(r) + \sum_{y=a,b} \bar{\Lambda}_y(-\mathbf{R},\mathrm{i}\omega) t_y(z), \tag{53}$$

$$\bar{t}_f(\mathbf{r},\mathrm{i}\omega) = t_f(r) + \sum_{y=a,b} t^*_y(z) \Lambda_y(\mathbf{R},\mathrm{i}\omega) \tag{54}$$

give the renormalized tunneling functions between the tip and the adatom, whose bare form, $t_f(r)$, is defined in equation (44). We also defined

$$\Lambda_x(\mathbf{R}) = \sum_{\mathbf{k}} \Lambda(k)\, \mathrm{e}^{\mathrm{i}\mathbf{k}\mathbf{R}},$$

$$\bar{\Lambda}_x(\mathbf{R}) = \sum_{\mathbf{k}} \bar{\Lambda}(k)\, \mathrm{e}^{\mathrm{i}\mathbf{k}\mathbf{R}}$$

as the Fourier transforms of $\Lambda(k)$ and $\bar{\Lambda}(k)$ (see equations (35) and (36)).

The self-energy correction to the localized electrons, $\Sigma_{ff}(\omega)$, as given in equation (14), is also dressed by the proximity of the STM tip and assumes the form

$$\Sigma_{ff}(\mathbf{r},\mathrm{i}\omega) = \Sigma_{ff}(\mathrm{i}\omega) + \Sigma^{(1)}_{ff}(\mathbf{r},\mathrm{i}\omega), \tag{55}$$

where

$$\Sigma^{(1)}_{ff}(\mathbf{r},\mathrm{i}\omega) = t_f(\mathbf{r})\bar{t}_f(\mathbf{r}) \sum_{\mathbf{k}} G_{cc}(k) \tag{56}$$

gives the contribution from the tip to leading order in t_f and t_x. In the presence of the STM tip, the Green's function of the localized electrons depends explicitly on the distance between the tip to the adatom,

$$G^{\mathrm{R}}_{ff,\sigma}(\mathrm{i}\omega) = \left[\mathrm{i}\omega - \epsilon_\sigma - \Sigma_{ff}(\mathbf{r},\mathrm{i}\omega)\right]^{-1} \tag{57}$$

which reflects the influence of the tip into the wavefunction of the localized states.

The imaginary part of the self energy, $\mathrm{Im}\Sigma^{(1)}_{ff}(\mathbf{r},\mathrm{i}\omega)$, renormalizes the level broadening $\Delta(\omega)$, defined in equation (21), due to the hybridization of the localized electrons with the electrons in the tip. In contrast with metallic hosts, which have a large DOS, in graphene the metallic tip can locally overwhelm the hybridization of the adatom with the nearby carbon atoms. In the situation where the level broadening becomes large enough as to overcome local correlation effects in the localized state, the tip might eventually lead to suppression of the local magnetism. This effect will be discussed in more detail in section 5.2.

Finally, other useful quantities are two off-diagonal Green's functions $G_{cx,\sigma}(\mathbf{p},\tau) = -\langle T[c(\tau)x^\dagger(0)]\rangle$, with $x = a, b$, which are given by

$$G_{cx,\sigma}(\mathbf{p},\mathbf{p}',\mathrm{i}\omega) = G^0_{cc}(p)\left[T^*_y(p',\mathbf{r}) + \bar{t}_f(\mathbf{r},\mathrm{i}\omega)\bar{\Gamma}_x(p',\mathbf{r})G_{ff,\sigma}(\mathrm{i}\omega)\bar{\Lambda}_x(p')\right] \tag{58}$$

and also

$$G_{cf,\sigma}(p) = G^0_{cc}(p)\bar{t}_f(\mathbf{r},\mathrm{i}\omega)G_{ff,\sigma}(\mathrm{i}\omega) \tag{59}$$

which are required for computing the differential conductance (see section 5.2.1).

5.1.1. Local density of states. Besides the localized state, the LDOS around the adatom is also affected by the presence of the STM tip. The LDOS nearby the impurity is also indirectly affected by the hybridization of the orbitals of the tip with the adatom localized orbital. For instance, for a magnetic adatom, the DOS is expected to be spin polarized on a given sublattice x,

$$\rho_{x,\sigma}(\mathbf{r},\omega) = -\frac{1}{\pi}\mathrm{Im}\sum_{\mathbf{p},\mathbf{p}'} G^{\mathrm{R}}_{xx,\sigma}(\mathbf{p},\mathbf{p}',\omega)\mathrm{e}^{\mathrm{i}(\mathbf{p}-\mathbf{p}')\mathbf{R}}, \tag{60}$$

where the diagonal Green's function $G_{xx,\sigma}(\mathbf{p},\mathbf{p}',\mathrm{i}\omega)$ is explicitly shown in equation (47). In a more explicit form

$$\rho_{x,\sigma}(\mathbf{r},\omega) = -\frac{1}{\pi}\mathrm{Im}\left[\sum_{\mathbf{p}} G^0_{xx}(p) + [\Gamma_x * \Lambda_x](\mathbf{r})\, G_{ff,\sigma}(\omega)\, [\bar{\Gamma}_x * \bar{\Lambda}_x](\mathbf{r}) + T_x(z)\bar{T}_x(z)\sum_{\mathbf{k}} G^0_{cc}(k)\right] \tag{61}$$

gives the LDOS per spin, where

$$[\Gamma_x * \Lambda_x](\mathbf{r}) \equiv \sum_{\mathbf{p}} \mathrm{e}^{\mathrm{i}\mathbf{p}\mathbf{R}}\, \Gamma_x(p,\mathbf{r})\Lambda_x(p), \tag{62}$$

$$[\bar{\Gamma}_x * \bar{\Lambda}_x](\mathbf{r}) \equiv \sum_{\mathbf{p}} \mathrm{e}^{-\mathrm{i}\mathbf{p}\mathbf{R}}\, \bar{\Gamma}_x(p,\mathbf{r})\bar{\Lambda}_x(p) \tag{63}$$

is the Fourier transform convoluted over the product of the $\Gamma(p,\mathbf{r})$ and $\Lambda_x(p)$ functions (and their respective conjugate forms), as defined in equations (35), (36) and (51), (52), while $T_x(z,\omega)$ is by definition $T(\mathbf{r},\omega)|_{\mathbf{R}=0}$ (see equation (48)), and hence independent of the horizontal distance between the tip and the adatom.

In figure 10 we show the topography maps for LDOS in the presence of the STM tip for both sublattices in the case of an adatom sitting on top of a carbon atom (top panels) and also for an adatom on an H site (lower panels). In those plots, we use the same set of parameters as before, $V = 1\,\mathrm{eV}$, $U = 1\,\mathrm{eV}$, $\mu = 0.1\,\mathrm{eV}$ and $\epsilon_0 = -0.5\,\mathrm{eV}$, and additionally the parameters $\alpha_D = 4\,\mathrm{eV}$ for the band width of the tip and $\epsilon_D = 2\,\mathrm{eV}$ for the Fermi energy of the tip. The tunneling parameters between the tip and the system where chosen to be $t_f = 0.02\,\mathrm{eV}$ and $t_a = t_b = 0.2\,\mathrm{eV}$. When the STM tip is weakly coupled to the impurity, the plots show basically the same qualitative features as the ones shown in figure 6 for the actual DOS on graphene in the absence of the STM tip. Due to the small DOS in the bath, additional features reflecting the suppression of the local moment are possible when the tip gets close to the adatom [22].

5.2. Tunneling current

The tunneling current from the tip is defined by [20]

$$I = -e\left\langle \frac{\mathrm{d}\hat{N}_c(t)}{\mathrm{d}t}\right\rangle, \tag{64}$$

where $\hat{N}_c = \sum_{\mathbf{k}\sigma} c^{\dagger}_{\mathbf{k}\sigma} c_{\mathbf{k}\sigma}$ is the number operator for the c electrons in the tip and e is the electron charge. The motion equation for this operator is

$$\partial_t \hat{N}_c = \mathrm{i}\left[H, \hat{N}_c\right],$$

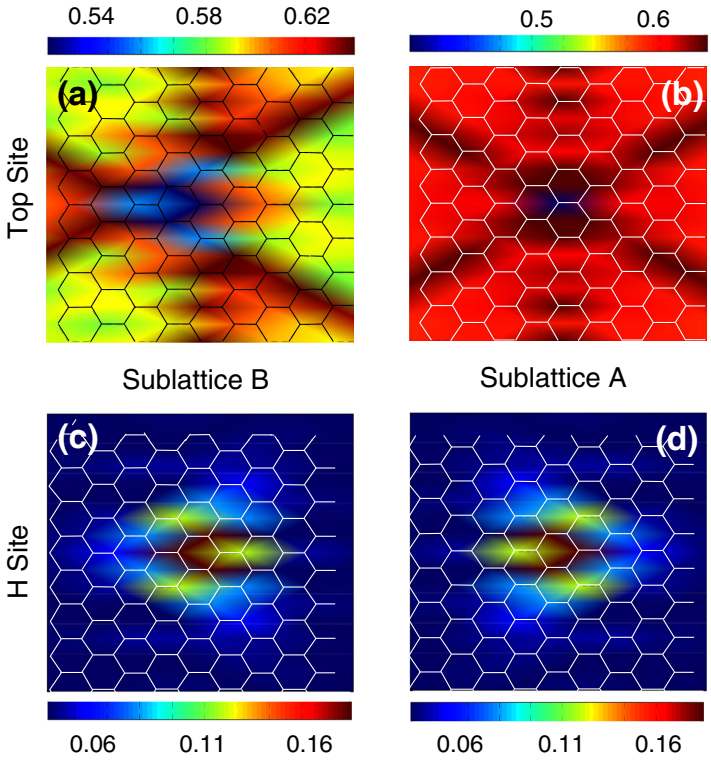

Figure 10. Energy integrated LDOS around the adatom (center) in the presence of an STM tip. (a) Scans for the same sublattice of the impurity and (b) for the opposite sublattice (top carbon site case). Scans for sublattice (c) A and (d) B, near an adatom sitting at the center of a honeycomb hexagon for some magnetic $m = 0$ angular momentum state (center).

where H is the full Hamiltonian defined in equation (45) including hopping matrix elements between the tip and the system. After a straightforward algebra, the total current follows from the sum of three different contributions that arise from tip tunneling processes to either sublattices A and B or else to the adatom localized state:

$$I = -2e\,\mathrm{Im}\int_{-\infty}^{\infty}\frac{\mathrm{d}\omega}{2\pi}\left[t_f(\mathbf{r})\sum_{\mathbf{k},\sigma}\mathrm{i}G^{<}_{cf,\sigma}(\mathbf{k},\omega)+\sum_{\mathbf{kp},\sigma}\sum_{x=a,b}t_{x,\mathbf{p}}(z)iG^{<}_{cx,\sigma}(\mathbf{k},\mathbf{p},\omega)\right], \tag{65}$$

where

$$G^{<}(t,t')\equiv \mathrm{i}\left\langle\psi^{\dagger}(t')\psi(t)\right\rangle, \tag{66}$$

$$G^{>}(t,t')\equiv -\mathrm{i}\left\langle\psi(t)\psi^{\dagger}(t')\right\rangle \tag{67}$$

are real time 'lesser' and 'greater' Green's functions, which should be distinguished from retarded (G^{R}) and advanced (G^{A}) ones, which are time ordered. If $A(\omega)=B(\omega)C(\omega)$, one may show that [36]

$$A^{<}(\omega)=B^{\mathrm{R}}(\omega)C^{<}(\omega)+B^{<}(\omega)C^{\mathrm{A}}(\omega) \tag{68}$$

in which case the total current can be written as

$$I = -2e\,\mathrm{Im}\int_{-\infty}^{\infty}\frac{\mathrm{d}\omega}{2\pi\,\mathrm{i}}\sum_{\mathbf{k}}\left[G_{cc}^{0\,\mathrm{R}}(k)\Sigma_{cc}^{<}(\mathbf{r},\omega)+G_{cc}^{0<}(k)\Sigma_{cc}^{\mathrm{A}}(\mathbf{r},\omega)\right], \tag{69}$$

where

$$\Sigma_{cc}(\mathbf{r},\mathrm{i}\omega)=\sum_{\mathbf{p}}\sum_{x=a,b}t_x(z)\bar{T}_x(z,\,p)+t_f(\mathbf{r})\bar{t}_f(\mathbf{r})\sum_{\sigma}G_{ff,\sigma}(\mathrm{i}\omega) \tag{70}$$

is the self-energy correction to the Green's function of the c-electrons in the tip,

$$G_{cc}(\mathbf{p},\mathbf{p}',\mathrm{i}\omega)=\left[(\mathrm{i}\omega-\epsilon_{\mathbf{p}})\delta_{\mathbf{p},\mathbf{p}'}-\Sigma_{cc}(\mathbf{r},\mathrm{i}\omega)\right]^{-1}. \tag{71}$$

The first term in equation (70) gives the self-energy contribution due to the graphene electrons, while the second one is the contribution from the adatom. Using the fluctuation dissipation theorem [36]

$$G^{<}(\omega)=\mathrm{i}f(\omega)A(\omega), \tag{72}$$

where $A(\omega)=-2\,\mathrm{Im}\,G^{\mathrm{R}}(\omega)$ is the spectral function, the total current is given by

$$I(\mathbf{r},\omega')=2\pi e\,t_a^2(z)\int_{-\infty}^{\infty}\mathrm{d}\omega\,\rho_t(\mathbf{r},\omega)\rho_c(\omega')\left[f(\omega)-f(\omega')\right], \tag{73}$$

where $f(\omega)=[\mathrm{e}^{\omega/T}+1]^{-1}$ is the Fermi distribution, ρ_c is the DOS at the STM tip,

$$\rho_c(\omega)=-\frac{1}{\pi}\sum_{\mathbf{k}}\mathrm{Im}\,G_{cc}^{0}(k), \tag{74}$$

and ρ_t is defined as

$$\rho_t(\mathbf{r},\omega)=-\frac{1}{\pi\,t_a^2(z)}\mathrm{Im}\Sigma_{cc}^{\mathrm{R}}(\mathbf{r},\omega). \tag{75}$$

This term has units of DOS, and accounts for the phases acquired by the electrons in the tunneling process between the tip and the localized state of the adatom. It can be conveniently rewritten in the following form:

$$\rho_t(\mathbf{r},\omega)=\rho_0(\omega)\left\{\nu(\omega)+\frac{\pi}{2}\rho_0(\omega)V^2\sum_{\sigma}\left[(\gamma\bar{\gamma}-q\bar{q})\,\mathrm{Im}\,G_{ff,\sigma}+(q\bar{\gamma}+\bar{q}\gamma)\mathrm{Re}\,G_{ff,\sigma}\right]\right\},$$

where

$$\nu(\omega)=-\frac{1}{\pi V\rho_0(\omega)}\,\mathrm{Im}\sum_{x=a,b}\bar{T}_x(\mathbf{R}=0,\omega). \tag{76}$$

$\rho_0(\omega)$ is the bare LDOS of graphene in the absence of the impurity and the tip, and $V\equiv\max\left(V_{x,i}\right)$, with $V_{x,i}$ the hybridization amplitudes of the adatom with the nearest carbon atoms, as defined in equation (22). The other parameter, q and its conjugate form, $\bar{q}$ are the Fano factors,

$$q(\mathbf{r},\omega)=\frac{1}{t_a(z)V}\,\frac{\mathrm{Re}\,t_f(\mathbf{r},\omega)}{\pi\rho_0(\omega)}, \tag{77}$$

$$\bar{q}(\mathbf{r},\omega)=\frac{1}{t_a(z)V}\,\frac{\mathrm{Re}\,\bar{t}_f(\mathbf{r},\omega)}{\pi\rho_0(\omega)}, \tag{78}$$

while

$$\gamma(\mathbf{r},\omega) = -\frac{1}{\pi V \rho_0(\omega)} \sum_{x=a,b} \mathrm{Im}\, \bar{\Lambda}_x(\mathbf{R},\omega), \tag{79}$$

$$\bar{\gamma}(\mathbf{r},\omega) = -\frac{1}{\pi V \rho_0(\omega)} \sum_{x=a,b} \mathrm{Im}\, \Lambda_x(\mathbf{R},\omega) \tag{80}$$

gives the corresponding damping factor. These factors characterize the Fano resonances in the differential conductance curves in the vicinity of a localized state.

5.2.1. Differential conductance. The Green's function of the localized electrons can be written in a more compact form as

$$G^{\mathrm{R}}_{ff,\sigma}(\omega) = \frac{\xi_\sigma - \mathrm{i}}{\xi_\sigma^2 + 1} \frac{1}{\mathrm{Im}\, \Sigma_{ff}(\mathbf{r},\omega)}, \tag{81}$$

where $\Sigma_{ff}(\mathbf{r},\omega)$ is the dressed self-energy of the localized electrons due to the proximity of the tip, as defined in equation (55), and $\xi_\sigma(\omega)$ is defined as

$$\xi_\sigma(\mathbf{r},\omega) = \frac{\omega - \epsilon_\sigma - \mathrm{Re}\, \Sigma_{ff}(\mathbf{r},\omega)}{\mathrm{Im}\, \Sigma_{ff}(\mathbf{r},\omega)} \tag{82}$$

The differential conductance follows by computing I/V_b in the limit of $V_b \equiv \omega' - \omega \to 0$. Since $df(\omega')/d\omega = -\delta(\omega')$ at zero temperature, the differential conductance can be written in the more standard form

$$\mathcal{G}(\mathbf{R},\omega_\mathrm{b}) = 2\pi e \rho_c(0) t_f^2(z) \rho_0(\omega_\mathrm{b}) \sum_\sigma \left\{ \nu(\omega_\mathrm{b}) + \left[\frac{q\bar{q} - \gamma\bar{\gamma} + (q\bar{\gamma} + \bar{q}\gamma)\xi_\sigma}{\xi_\sigma^2 + 1} \right] \right\}, \tag{83}$$

where ω_b is the bias voltage. The first term in parentheses defines the dc due to the DOS in graphene. The second one is explicitly defined in terms of the Fano parameters and gives the contribution due to the presence of the magnetic adatom.

The experimental detection of a localized state with STM tips is based on the principle of quantum interference between the two different hybridization paths the electrons can take when they tunnel from the impurity to the localized state. In one way, the electrons can tunnel directly to the localized state. On the other, they can also tunnel to the host material (graphene) and then hybridize with the localized orbital. The signature of such interference appears in the differential conductance curves in the form of a Fano resonance. In graphene, the electrons have additional sublattice quantum numbers which may give rise to additional interference effects, depending on the position of the adatom relative to the two different sublattices. In the case where the adatom sits in the center of the honeycomb hexagon, for a given sublattice, there are three different paths the electrons in graphene can take to hybridize with the adatom. Destructive interference between the different paths in a given sublattice can suppress the Fano character of the resonance and change the shape of the dc curves.

When the tip is above the adatom ($R = 0$), the conjugate forms $q = \bar{q}$ and $\gamma = \bar{\gamma}$ in equations (77)–(80) are the same. In the simplest scenario, where an adatom sits on top of a

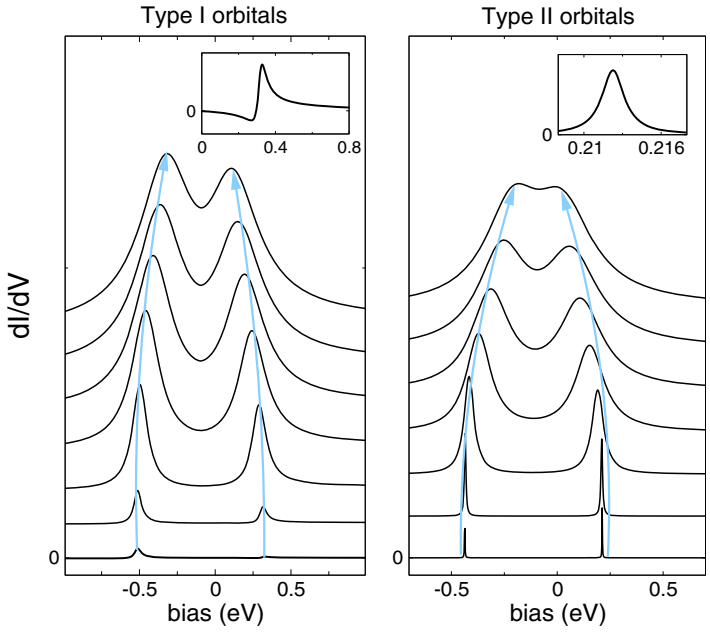

Figure 11. Differential conductance induced by the adatom versus bias when the tip is right above the adatom ($\mathbf{R} = 0$) for $m = 0$ states. The different curves are shifted vertically. Left: type one orbitals, for adatoms that sit on top of carbon site; right: type II orbitals at S or H sites ($m = 0$). See details in the text. (a), (b) $t_a = t_b = 0.15$ eV and $t_f/t_a = 1.6$, 1.5, 1.35, 1.1, 0.7, 0.25 and 0.1 (inset), from top to bottom.

carbon atom, say on site A, the Fano factor is defined explicitly in terms of the self-energy for orbitals of type I, Re $\Sigma^{\rm I}_{ff}(\omega) = \omega[Z_I^{-1}(\omega) - 1]$, as given in equation (27), namely

$$q^{\rm A}(0,\omega) = \frac{V_c + (t_a(z)/V)\,\mathrm{Re}\,\Sigma^{\rm I}_{ff}(\omega)}{\pi t_a(z) V \rho_0(\omega)}\,. \tag{84}$$

The damping in this case is $\gamma^{\rm A} = 1$, by noticing that integrals with off diagonal matrix elements of the Green's function, such as $\sum_{\mathbf{k}} G_{ab} = 0$. In a different scenario, for adatoms of type II, which sit either in S or H sites and possess orbitals with C_{3v} point group symmetry, as discussed in section 3, the hybridization matrix elements have the form $V_{b,\mathbf{p}} = \pm V\phi_{\mathbf{p}}$ and $V_{a,\mathbf{p}} = V\phi^*_{\mathbf{p}}$, in which case one can easily check that $\Lambda(\mathbf{R} = 0, \omega) = \sum_{x,y=a,b}\sum_{\mathbf{k}} G_{xy} V_{y,\mathbf{p}} = 0$. In that case,

$$q^{\rm II}(0,\omega) = V_c/\left[\pi t_a(z) V \rho_0(\omega)\right] \tag{85}$$

and $\gamma^{\rm II} = 0$. In the more generic case, for type I orbitals (the ones which are not C_{3v} invariant) that sit on H or S sites, the damping factor γ interpolates between 0 and $N_{\rm s} = 1, 2$, the number of sublattices the adatom effectively hybridizes.

As the usual theory of Fano resonances [21], when $q/\gamma \gg 1$, the dc curve has the form of a peak, whereas in the opposite limit, for $q/\gamma \ll 1$ it is shows a dip. In figure 11 we show the DC induced by the presence of the adatom for $m = 0$ orbitals in two cases: when it sits on top of a carbon site (left panels) and also when it sits at an H site (right panels). In panels (a) and (b) we assume a fixed set of parameters and change the ratios t_f/t_a for a given fixed value of $t_a = 0.15$ eV. For $t_f/t_a \lesssim 0.1$, the DC curve of type I orbitals has a Fano shape, whereas for all type II orbitals the Fano resonance is suppressed (see insets of figure 11).

The evolution of the separation of the peaks can be rigorously analyzed within the single orbital model for the case of $m = 0$ orbitals. The increase of t_f leads to a gradual suppression of the local magnetic moment, and as a consequence to a decrease in the separation of the two peaks. In the $m \neq 0$ case, a significant suppression of the local moment by the STM tip is also accompanied by a redistribution of the charge between different orbitals contained in given irreducible representation.

6. Conclusion

Unlike the case of metallic hosts, in graphene the symmetry of the localized orbital has clear fingerprints in the LDOS nearby the adatom whenever the adatom, hybridizes with two or more carbon atoms. We showed that the real and momentum space STM scanning maps can reveal not only the position of the adatom with respect to the sublattices but can also indicate the orbital symmetry of the localized state and possibly its magnetic state.

We have described in detail how sublattice quantum numbers in combination with orbital symmetry effects influence the Fano resonances in the differential conductance nearby the adatom. To illustrate the effect, we analyzed the problem in the single orbital picture, which is valid for orbitals in one-dimensional irreducible representations (such as s-wave, d_{zz}-wave, etc), as well as in the more interesting case of two-dimensional irreducible representations, such as in the doublets $(d_{x^2-y^2}, d_{xy})$, $(f_{x(x^2-3y^2)}, f_{y(3y^2-x^2)})$, etc, when the energy separation of the orbitals in the doublet state, driven for instance by charge and spin polarization effects, is large compared to the level broadening. In the presence of small Jahn–Teller distortion effects, which freeze charge fluctuations between the polarized orbitals and hence break the point group symmetry of the underlying crystal, those different orbitals may leave explicit fingerprints in the LDOS. Those distortions can occur either spontaneously, when adatoms are randomly adsorbed on graphene, or else through the application of strain.

Acknowledgments

We acknowledge P M Goldbart, E Andrei, H Manoharan, A Balatsky, K Sengupta and M Vojta for discussions. BU acknowledges partial support from DOI grant DE-FG02-07ER46453 at the University of Illinois. LY and SWT acknowledge financial support from NSF under grant DMR0847801 and from the UC-Lab FRP under award number 09-LR-05-118602. AHCN acknowledges DOE grant DE-FG02-08ER46512 and NRF-CRP award 'Novel 2D materials with tailored properties beyond graphene' (R-144-000-295-281).

Appendix. Exact Green's functions

At the mean field level, the Green's functions described in section 4 can be written in an exact form by solving the equations of motion for the fermionic operators $a_{\mathbf{k},\sigma}$, $b_{\mathbf{k},\sigma}$, $c_{\mathbf{p},\sigma}$ and f_σ. After cumbersome but straightforward algebra, the final expressions are

$$G_{xy,\sigma}(\mathbf{p}, \mathbf{p}', \mathrm{i}\omega) = \delta_{\mathbf{p},\mathbf{p}'} G^0_{xy}(p) + \Gamma_x(p, \mathbf{r})\Lambda_x(p) G_{ff,\sigma}(\mathrm{i}\omega)\bar{\Lambda}_y(p')\bar{\Gamma}_y(p', \mathbf{r}) + \sum_{\mathbf{k}\mathbf{k}'} T_{x,\mathbf{k}'}(\mathbf{r}, p) G_{cc}(\mathbf{k}, \mathbf{k}', \mathrm{i}\omega)\bar{T}_{y,\mathbf{k}'}(\mathbf{r}, p'), \quad \text{(A.1)}$$

$$G_{cx,\sigma}(\mathbf{p},\mathbf{p}',\mathrm{i}\omega)=\sum_{\mathbf{k}}G_{cc}(\mathbf{p},\mathbf{k}',\mathrm{i}\omega)\left[\bar{T}_{x,\mathbf{k}}(\mathbf{r},p')+\bar{t}_{f,\mathbf{k}}\bar{\Gamma}_{x,\mathbf{p}'}G_{ff,\sigma}(\mathrm{i}\omega)\bar{\Lambda}_x(p')\right] \tag{A.2}$$

and

$$G_{cf,\sigma}(\mathbf{p}',\mathrm{i}\omega)=\sum_{\mathbf{p}}G_{cc}(\mathbf{p},\mathbf{p}',\mathrm{i}\omega)\bar{t}_{f,\mathbf{p}}(\mathbf{r})G_{ff,\sigma}(\mathrm{i}\omega), \tag{A.3}$$

where $p\equiv(\mathbf{p},\mathrm{i}\omega)$. The quantities $\Lambda_x(p)$ and $\bar{\Lambda}_x(p)$ have the same definitions as before (see equations (35) and (36)), whereas

$$T_{\mathbf{p}',x}(\mathbf{r},p)\equiv\sum_{y=a,b}G^0_{xy}(p)t_{y,\mathbf{p},\mathbf{p}'}(\mathbf{r}), \tag{A.4}$$

$$\bar{T}_{\mathbf{p}',x}(\mathbf{r},p)\equiv\sum_{y=a,b}t^*_{y,\mathbf{p},\mathbf{p}'}(\mathbf{r})G^0_{yx}(p)\,. \tag{A.5}$$

The Green's function of the c-electrons is defined as

$$G_{cc}(\mathbf{p},\mathbf{p}',\mathrm{i}\omega)=\left[(\mathrm{i}\omega-\epsilon_{\mathbf{p}})\delta_{\mathbf{p}\mathbf{p}'}-\Sigma_{cc,\mathbf{p}\mathbf{p}'}(z,\mathrm{i}\omega)\right]^{-1}, \tag{A.6}$$

where Σ_{cc} is the self-energy for the electrons in the tip due to hybridization effects with the electrons in graphene only,

$$\Sigma_{cc,\mathbf{p}\mathbf{p}'}(z,\mathrm{i}\omega)=\sum_{\mathbf{k}}\sum_{x=a,b}t_{x,\mathbf{p}}(z)\bar{T}_{\mathbf{p}',x}(z,k). \tag{A.7}$$

The Green's function of the f-electrons is given by

$$G_{ff,\sigma}(\mathrm{i}\omega)=\left[\mathrm{i}\omega-\epsilon_\sigma-\Sigma_{ff}(\mathbf{r},\mathrm{i}\omega)\right]^{-1}, \tag{A.8}$$

where $\Sigma_{ff}(\mathbf{r},\mathrm{i}\omega)=\Sigma_{ff}(\mathrm{i}\omega)+\Sigma^{(t)}_{ff}(\mathbf{r},\mathrm{i}\omega)$ is the corresponding self-energy, with

$$\Sigma^{(t)}_{ff}(\mathbf{r},\mathrm{i}\omega)=\sum_{\mathbf{k}\mathbf{k}'}t_{f,\mathbf{k}}(\mathbf{r})G_{cc}(\mathbf{k},\mathbf{k}',\mathrm{i}\omega)\bar{t}_{f\mathbf{k}'}(\mathbf{r}) \tag{A.9}$$

as the contribution of the tip. The other quantities include the renormalized hybridization of the tip with the adatom

$$t_{f,\mathbf{p}}(\mathbf{r},\mathrm{i}\omega)=t_{f,\mathbf{p}}(r)+\sum_{\mathbf{k}}\sum_{y=a,b}\bar{\Lambda}_y(k)t_{y,\mathbf{k}\mathbf{p}}, \tag{A.10}$$

$$\bar{t}_{f,\mathbf{p}}(\mathbf{r},\mathrm{i}\omega)=t_{f,\mathbf{p}}(r)+\sum_{\mathbf{k}}\sum_{y=a,b}t^*_{y,\mathbf{k}\mathbf{p}}\Lambda_y(k) \tag{A.11}$$

and

$$\Gamma_x(p)=1+\sum_{\mathbf{k}\mathbf{k}'}\bar{t}_{f,\mathbf{k}}(\mathbf{r},\mathrm{i}\omega)G_{cc}(\mathbf{k},\mathbf{k}',\mathrm{i}\omega)\frac{T_{\mathbf{k}',x}(\mathbf{r},p)}{\Lambda_x(p)},$$

$$\bar{\Gamma}_x(p)=1+\sum_{\mathbf{k}\mathbf{k}'}\frac{\bar{T}_{\mathbf{k}',x}(\mathbf{r},p)}{\bar{\Lambda}_x(p)}G_{cc}(\mathbf{k},\mathbf{k}',\mathrm{i}\omega)t_{f,\mathbf{k}}(\mathbf{r},\mathrm{i}\omega)$$

which are vertex corrections that appear in equations (A.1) and (A.2).

References

[1] Novoselov K S, Geim A K, Morozov S V, Jiang D, Katsnelson M I, Grigorieva I V, Dubonos S V and Firsov A A 2005 *Nature* **438** 197
[2] Zhang Y, Tan Y-W, Stormer H L and Kim P 2005 *Nature* **438** 201
[3] Castro Neto A H, Guinea F, Peres N M R, Novoselov K S and Geim A K 2009 *Rev. Mod. Phys.* **81** 109
[4] Eigler D M and Schweizer E K 1990 *Nature* **344** 524
[5] Uchoa B, Kotov V N, Peres N M R and Castro Neto A H 2008 *Phys. Rev. Lett.* **101** 026805
[6] Sengupta K and Baskaran G 2008 *Phys. Rev.* B **77** 045417
[7] Stolyarova E, Rim K T, Ryu S, Maultzsch J, Kim P, Brus L E, Heinz T F, Hybertsen M S and Flynn G W 2007 *Proc. Natl Acad. Sci. USA* **104** 9209
[8] Rutter G M, Crain J N, Guisinger N P, Li T, First P N and Stroscio J A 2007 *Science* **317** 219
[9] Brar V, Zhang Y, Yayon Y, Ohta T, McChesney J L, Bostwick A, Rotenberg E, Horn K and Crommie M F 2007 *Appl. Phys. Lett.* **91** 122102
[10] Ishigami M, Chen J H, Cullen W G, Fuhrer M S and Williams E D 2007 *Nano Lett.* **7** 1643
[11] Zhang Y, Brar V W, Wang F, Girit C, Yayon Y, Panlasigui M, Zettl A and Crommie M F 2008 *Nature Phys.* **4** 627
[12] Geringer V, Liebmann M, Echtermeyer T, Runte S, Schmidt M, Rückamp R, Lemme M C and Morgenstern M 2009 *Phys. Rev. Lett.* **102** 076102
[13] Li G, Luican A and Andrei E Y 2009 *Phys. Rev. Lett.* **102** 176804
[14] Xue J, Sanchez-Yamagishi J, Bulmash D, Jacquod P, Deshpande A, Watanabe K, Taniguchi T, Jarillo-Herrero P and LeRoy B J 2011 *Nature Mater.* **10** 282–5
[15] Deshpande A, Bao W, Miao F, Lau C N and Leroy B J 2009 *Phys. Rev.* B **79** 205411
[16] Brihuega I, Mallet P, Bena C, Bose S, Michaelis C, Vitali L, Varchon F, Magaud L, Kern K and Veuillen J Y 2008 *Phys. Rev. Lett.* **101** 206802
[17] Levy N, Burke S A, Meaker K L, Panlasigui M, Zettl A, Guinea F, Castro Neto A H and Crommie M F 2010 *Science* **329** 544
[18] Brar V W *et al* 2011 *Nature Phys.* **7** 43–7
[19] Tersoff J and Hamann D R 1985 *Phys. Rev.* B **31** 805
[20] Plihal M and Gadzuk J W 2001 *Phys. Rev.* B **63** 085404
[21] Fano U 1961 *Phys. Rev.* **124** 1866
[22] Uchoa B, Yang L, Tsai S-W, Peres N M R and Castro Neto A H 2009 *Phys. Rev. Lett.* **103** 206804
[23] Saha K, Paul I and Sengupta K 2010 *Phys. Rev.* B **81** 165446
[24] Wehling T O, Dahal H P, Lichtenstein A I, Katsnelson M I, Manoharan H C and Balatsky A V 2010 *Phys. Rev.* B **81** 085413
[25] Uchoa B, Rappoport T G and Castro Neto A H 2011 *Phys. Rev. Lett.* **106** 016801
[26] Liu X *et al* 2011 *Phys. Rev.* B **83** 235411
[27] Coqblin B and Blandin A 1968 *Adv. Phys.* **17** 281
[28] Leenaerts O, Partoens B and Peeters F M 2008 *Phys. Rev.* B **77** 125416
[29] Chan K T, Neaton J B and Cohen M L 2008 *Phys. Rev.* B **77** 235430
[30] Krasheninnikov A V, Lehtinen P O, Foster A S, Pyykkö P and Nieminen R M 2009 *Phys. Rev. Lett.* **102** 126807
[31] Anderson P W 1961 *Phys. Rev.* **124** 41
[32] Slizovskiy S and Betouras J J 2012 *Phys. Rev.* B **86** 125440
[33] Wehling T O, Balatsky A V, Katsnelson M I, Lichtenstein A I and Rosch A 2010 *Phys. Rev.* B **81** 115427
[34] Jacob D and Kotliar G 2010 *Phys. Rev.* B **82** 085423
[35] Elbo T *et al* 2013 *Phys. Rev. Lett.* **110** 136804
[36] Kadanoff L P and Baym G 1962 *Quantum Statistical Mechanics* (New York: Benjamin)